Environmental Science & Technology

pubs.acs.org/est

Article

Nontarget Analysis of Legacy and Emerging PFAS in a Lithium-Ion Power Battery Recycling Park and Their Possible Toxicity Measured Using High-Throughput Phenotype Screening

Zenghua Qi, Yutian Cao, Dan Li, Chenguang Wu, Kaihan Wu, Yuanyuan Song, Zeji Huang, Hemi Luan,* Xiaojing Meng, Zhu Yang, and Zongwei Cai*

Cite This: *Environ. Sci. Technol.* 2024, 58, 14530−14540

Read Online

ACCESS | Metrics & More | Article Recommendations | Supporting Information

ABSTRACT: Driven by the global popularity of electric vehicles and the shortage of critical raw materials for batteries, the spent lithium-ion power battery (LIPB) recycling industry has exhibited explosive growth in both quantity and scale. However, relatively little information is known about the environmental risks posed by LIPB recycling, in particular with regards to perfluoroalkyl and polyfluoroalkyl substances (PFAS). In this work, suspect screening and nontarget analysis were carried out to characterize PFAS in soil, dust, water and sediment from a LIPB recycling area. Twenty-five PFAS from nine classes were identified at confidence level 3 or above, including 13 legacy and 12 emerging PFAS, as well as two ultrashort-chain PFAS. Based on the target analysis of 16 PFAS, at least nine were detected in each environmental sample, indicating their widespread presence in a LIPB recycling area. Perfluorodecanoic acid, perfluorooctanesulfonic acid and trifluoromethanesulfonamide showed significant differences in the four phenotypic parameters (growth, movement, survival and fecundity) of *Caenorhabditis elegans* and were the most toxic substances in all target PFAS at an exposure concentration of 200 μM. Our project provides first-hand information on the existence and environmental risk of PFAS, facilitating the formulation of regulations and green development of the LIPB recycling industry.

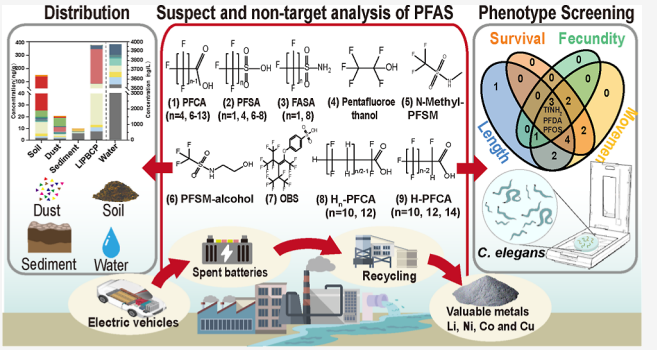

KEYWORDS: *PFAS, lithium-ion power batteries, recycling, nontarget analysis, phenotypic screening*

1. INTRODUCTION

As the popularity of electric vehicles starts to soar, so does the volume of lithium-ion power batteries (LIPBs) that once powered those cars. In order to cope with the upcoming peak in the number of retired LIPBs, and the problems around the insufficient supply of the transition metals Co, Ni and Li and their rising prices in the battery manufacturing process, countries around the world are vigorously promoting and developing the lithium-ion power battery (LIPB) recycling industry. In 2022, China recycled 102,000 tons of spent LIPBs and this is expected to reach 570,000 tons in 2025.[1] The European Parliament and the Council stated mandatory requirements for the recovery of spent LIPBs in regulations issued on July 12, 2023.[2] At this stage, recovery of critical raw materials (in particular metals) through recycling has generated considerable economic and ecological value. At the same time, a number of environmental problems caused by the "recycling tide" of LIPBs have become increasingly prominent.

In the process of dismantling and recycling LIPBs, a variety of heavy metals from cathode materials, fluorine-containing electrolytes in the electrolyte, and toxic and harmful substances such as organic solvents will continue to be released into areas and the surrounding environment, which will cause serious harm to people's health.[3,4] Although research and understanding of the pollution characteristics and health risks of pollutants in LIPB recycling sites are still very limited, it can be inferred that persistent (in)organic fluorinated chemicals are representative pollutants that should be focused on in recycling sites, based on LIPBs' components, process flow and toxic effects.[5] Rensmo *et al.* demonstrated the possibility of perfluoroalkyl and polyfluoroalkyl substance (PFAS) formation and release during LIPB recycling with respect to battery composition and the recycling process (pyrometallurgy, hydrometallurgy), and highlighted the urgent need to investigate emissions of fluorinated substances during LIPB

Received: April 10, 2024
Revised: June 18, 2024
Accepted: July 12, 2024
Published: July 17, 2024

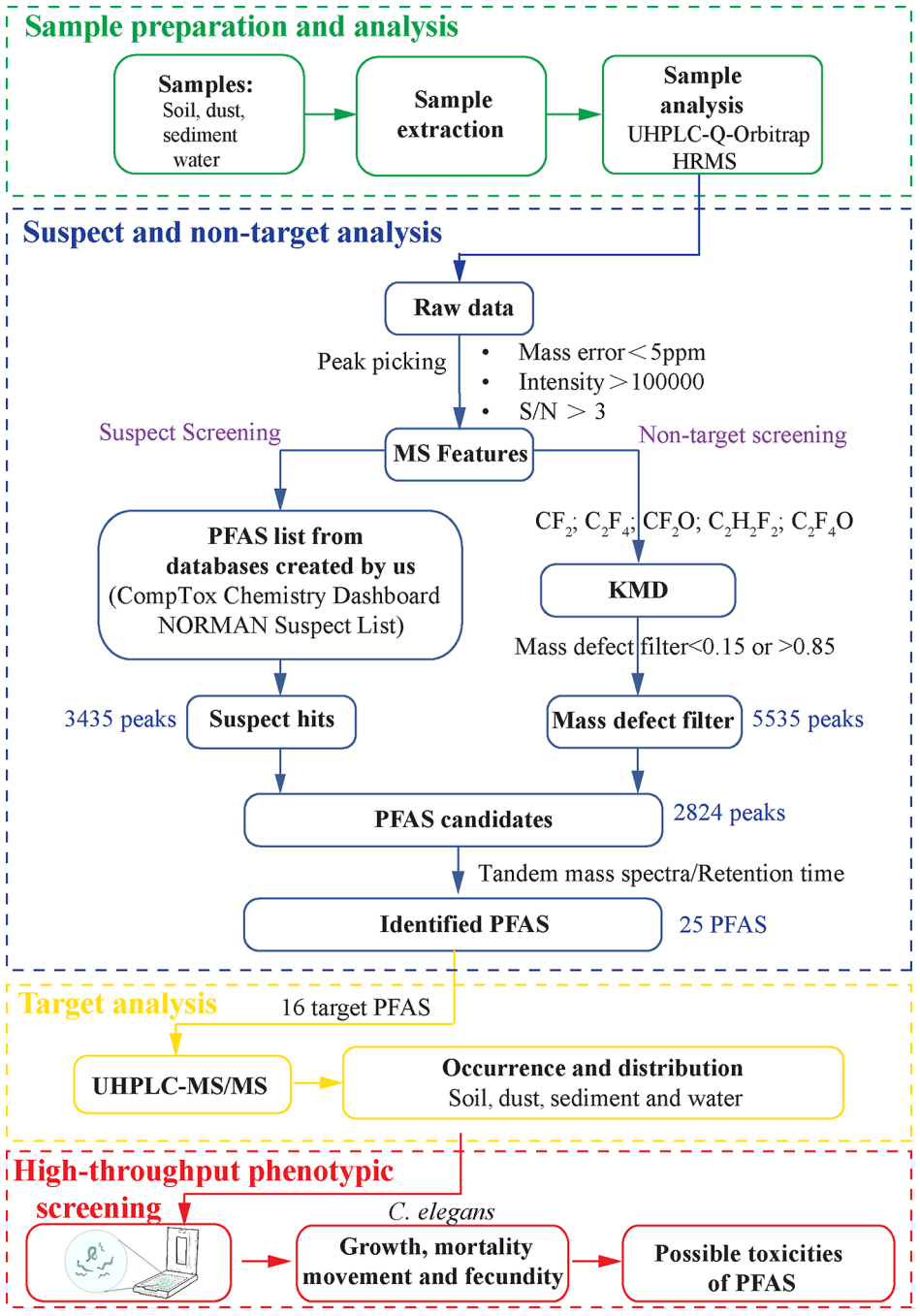

Figure 1. Workflow for integration of nontarget analysis and high-throughput phenotypic screening.

recycling.[6] PFAS have good thermal and chemical stability for reducing the surface tension of liquids and surfaces in the electrodes, binder, electrolyte (and additives), and separator.[7] During the recycling and disposal processes of LIPBs, PFAS may be released either directly or indirectly from the components. Notably, PFAS are easy to migrate and accumulate in different environmental media and organisms and can pose a threat to human health and ecosystem security. However, little information is known about the potential emission and occurrence of PFAS in LIPB recycling areas.

At present, the number of PFAS used in industrial production has exceeded 10,000 with various headgroups and properties. They may transform into one another in the environment, which poses significant difficulties for their detection when only depending on target analysis.[8] High-resolution mass spectrometry (HRMS), utilizing instruments such as Orbitrap and quadrupole time-of-flight mass spectrometers, has emerged as a powerful tool for identifying known and unknown PFAS.[9−11] In the context of PFAS screening, HRMS complements three common strategies: suspect screening, homologue-based screening, and fragment-based nontarget screening.[12] The wide mass range, high-resolution capabilities, and accurate mass measurements of HRMS allow for the comprehensive analysis of PFAS and facilitate their identification in various environmental samples.[13] In addition to the need to understand the exposure level of PFAS, it is very important to identify their toxicities when estimating their health risk. The existing high-throughput

https://doi.org/10.1021/acs.est.4c03552
Environ. Sci. Technol. 2024, 58, 14530−14540

toxicity screening methods mainly rely on a few isolated molecular targets, which are hard to screen and, ultimately, identify numerous PFAS, in particular novel PFAS obtained from nontarget analysis. Recently, it was shown that *Caenorhabditis elegans* (*C. elegans*) is an ideal model organism to evaluate both the ecological and health risks caused by environmental hazards.[14,15] Therefore, high-throughput phenotypic screening of *C. elegans* combined with nontarget analysis shows great potential for assessing the ecological and health risks from pollutants with multiple monomers.

To address the paucity of information on the occurrence of PFAS and their environmental risks, we first used the suspect and nontarget approach with HRMS to identify emerging and legacy PFAS in soil, dust, water and sediment from a recycling area. Subsequently, the distribution of PFAS in different media was investigated using target analysis. Finally, we assessed the multiple toxicities of PFAS using automatic high-throughput phenotypic screening.

2. MATERIALS AND METHODS

2.1. Chemicals and Reagents. Based on the results of nontargeted analysis, 17 commercially available PFAS standards and 9 isotope-labeled internal standards (ILISs) were purchased from three companies: Wellington Laboratories (Guelph, Ontario, Canada), ANPEL Laboratory Technologies (Shanghai, China) and Tokyo Chemical Industry (Tokyo, Japan) (Tables S1 and S2). Ammonium acetate (NH_4OAc, purity ≥99.9%) was purchased from Sigma-Aldrich (Stockholm, Sweden) and Ammonium Hydroxide (NH_4OH, purity 28−30% in water) was purchased from Thermo Fisher Scientific (Hampton, NH, USA). Methanol was purchased from Merck (Darmstadt, Germany). Milli-Q water was obtained from an ultrapure water purification system (Millipore, Billerica, MA, USA). The organic reagents used in the experiment were all high-performance liquid chromatography (HPLC) grade.

2.2. Study Area and Sample Collection. In this study, a large LIPB recycling park located in the southeast of Guangdong Province, China, was selected as the study site. This recycling park was opened in 2018 and covers an area of about 7 ha, with a maximum annual recovery capacity of about 200,000 tons. This recycling park can provide power battery performance testing, gradient utilization and valuable metal (Li, Ni, Co, Cu and Al) recycling services. The main type of spent lithium-ion batteries at the selected recycling park is ternary lithium battery containing valuable metals such as Li, Ni, Co, Cu and Al. Hydrometallurgy-dominant recycling processes are used for critical raw material separation and collection at this studied area (Figure S1).

From September 2022 to September 2023, we collected a variety of environmental samples from nine different areas of the site and, in total, collected 27 samples (three duplicate samples per sample site), including 18 topsoil samples, three dust samples, three sediment sample and three water sample. Figure S2 and Table S3 show the sampling location map, sample information and abbreviation about all samples collected, respectively. At the same time, the soil and surface water of the natural park 4 km away from the LIPB recycling area in the upwind position were collected as control samples. Surface water was collected using a stainless-steel sampler and placed in a 1 L high-density polyethylene container. Sediments were collected using a grab sampler, soil samples were collected using a shovel, and dust and powder samples were collected using a clean disposable brush and stored in a PE plastic bag. To trace the source of PFAS in environmental media, we also collected the LIPB crushing powder (LIPBCP) used in the recovery process. To avoid cross-contamination, the sampling tools and containers were prerinsed with Milli-Q water and methanol before sampling, and all samples were stored in PP containers. The samples were sealed with ice bags and transported as quickly as possible. After arriving at the laboratory, the samples were stored at −20 °C until analysis.

2.3. Suspect and Nontarget Screening of PFAS. The integral suspect and nontarget analysis flowchart is shown in Figure 1. The collected samples were pretreated within 1 week. Soil and dust samples were weighed and extracted with 0.1% NH_4OH·MeOH solution. After multiple ultrasonic centrifugation cycles, an ENVI-Carb SPE column was used for extraction. The eluent was MeOH. After extraction, it was concentrated using nitrogen blowing until redissolved. The sediment needed to be freeze-dried before extraction. The extract was 100 mM CH_3COONH_4·MeOH solution and was first concentrated using nitrogen blowing and then solid phase extraction. After filtration, the water sample was extracted using a HLB column, eluted with 0.1% NH_4OH·MeOH solution, concentrated using nitrogen blowing, redissolved with methanol, and filtered through a 0.22 μm nylon membrane. In addition, LIPBCP was pretreated in a similar way to soil and dust samples. Text S1 provides detailed information on the sample pretreatment method.

Sample analysis was carried out using a Dionex UltiMate 3000 HPLC coupled to a Q Exactive Orbitrap mass spectrometer (Thermo Fisher Scientific, MA, USA) with an ESI source operated in negative ion mode. The negative ion electrospray voltage was 2500 V. The gas flows were 40, 10, and 0 arb. for shear gas, aux gas, and sweet gas, respectively, and the temperatures of the ion transfer pipe and gasifier were 320 and 300 °C respectively. The MS/MS analysis was carried out in data-dependent acquisition mode with normalized collision energy settings (CE %) of 10, 20, and 40. Chromatographic separations were achieved using a Hypersil Gold C18 (Thermo Fisher Scientific, 1.9 μm, 2.1 × 100 mm). The mobile phase consisted of water with 5 mM ammonium acetate (solvent A) and methanol (solvent B). The flow rate was 300 μL/min, and the autosampler and column oven temperatures were maintained at 10 and 35 °C respectively. The binary solvent elution gradient was optimized at 10% B for 1 min, 10−70% B for 6 min, 70−95% B for 14 min and then held at 95% B for 7 min. The column was equilibrated for 4 min at 10% B between injections.

The process of suspect and nontarget screening of PFAS is in line with previous studies with some modification.[9] In brief, the raw data were preprocessed using Compound Discoverer 3.2 (Thermo Fisher Scientific, San Jose, CA, US) for peak picking. Suspect screening was carried out using a list of PFAS from our in-house PFAS database, which were collected from the NORMAN Suspect List Exchange and the US EPA CompTox Chemistry Dashboard. For nontarget screening, the extracted peaks with mass defects >0.85 or <0.15 were retained. Potential PFAS homologues were identified by mass differences in CF_2, C_2F_4, CF_2O, $C_2H_2F_2$, and C_2F_4O units among the exact mass of peaks by using the *nontarget* package.[16] In addition, the retention time (RT) of each peak should increase as the mass increases for the homologues in each homologue. The remained peaks were identified by comparing the accurate mass and MS/MS spectra in the in-

https://doi.org/10.1021/acs.est.4c03552
Environ. Sci. Technol. 2024, 58, 14530−14540

house PFAS database, and the RT of commercially available standard compounds. PFAS identification confidence levels were assigned following the criteria established in previous study.[17]

2.4. Quantifying the PFAS in the Soil, Dust, Water and Sediment from the Lithium-Ion Power Battery Recycling Area. Of the PFAS identified by nontargeted analysis, as some of them did not match authentic standard products, we analyzed 16 PFAS that could be purchased for the ultrahigh performance liquid chromatography tandem triple quadrupole mass spectrometry system. For ultrashort chain PFAS trifluoromethanesulfonic acid (TFMS) and trifluoromethanesulfonamide ($TfNH_2$), $^{18}O_1$−PFHxS and $^{13}C_3$−PFOS were selected as internal standards because there were no commercially available ILISs. After weighing all the soil, dust and sediment samples, a mixed standard containing nine ILISs was added to them, and the ILISs were added to the filtered water after filtration, so that the ILIS concentration of each sample was 4 μg/L. Three parallel samples were set at each point to minimize the influence of environmental factors on the experimental results.

An Dionex UltiMate 3000-TSQ Endura UHPLC-MS/MS system (Thermo Fisher Scientific) and XBridge BEH C18 XP Column (10 × 2.1 mm, 2.5 μm) were used for chromatographic separation at 40 °C. Briefly, the mobile phase of the instrument used (A) HPLC grade methanol and (B) 5 mM ammonium acetate modified LC-MS grade water as the binary gradient mobile phase, the flow rate was 300 μL/min, and the sample injection volume was 5 μL. Mass spectrometric detection was carried out using a TSQ Endura triple quadruple mass spectrometer with an electrospray ionization source. The parameters of the mass spectrometer were set as follows: capillary temperature was 320 °C, vaporizer temperature was 350 °C, sheath gas was set at 35 (arb.), auxiliary gas at 10 (arb.). The samples were analyzed with SRM in negative electrospray ionization mode (ESI-). Tables S4−S6 provide the details of the instrument parameters of the target PFAS and its corresponding ILISs. Thermo Scientific Xcalibur was used for data acquisition and processing analysis. Quality assurance and quality control of target analysis detection can be found in the Supporting Information (Text S2). Tables S7−S10 provide detailed information on the matrix spiked recovery, the method detection limit, the method quantitation limit, and blank level for each sample.

2.5. High-Throughput Phenotypic Screening of PFAS Using *C. elegans*. The *C. elegans* N2 wild-type worm was obtained from the Caenorhabditis Genetics Center. All nematodes were maintained in a standard nematode growth medium inoculated with *E. coli* OP50 at 20 °C using the standard culture protocol.[18] For each PFAS substance, the nematodes at the L4 stage were randomly divided into four exposure groups, each with 60 worms (30 per plate): a control group (C-group), a low PFAS dosage group (L-group, 200 μM), a medium dosage group (M-group, 600 μM), and a high dosage group (H-group, 1200 μM). In order to observe the long-term effects of PFAS on *C. elegans* and facilitate the observation of the number of offspring, L4 stage nematodes were specifically exposed to 15 PFAS for 96 h, and sterilized OP50 was added daily during the exposure to maintain the normal activity of the nematodes.

After PFAS exposure, all nematodes were transferred to 5.5 cm plates coated with 0.1% agar gel. Fifteen PFAS substances, a total of 120 plates of nematodes, were obtained, and then scanned using an Epson Perfection V850 Pro Scanner (Seiko Epson Corporation, Japan) with optional SilverFast8 software. To have sufficient clarity and imaging time, the image was taken using a 16-bit grayscale with a resolution of 6400 dpi. This mode was sufficient to observe nematodes in different periods and scanning could take place twice within 10 min. The size of the generated image was verified using a standard ruler placed on the scanner.

The methods used for *C. elegans* image capture and statistics in this study are in line with Mathew's method, albeit with some modifications.[19] Briefly, we ran the "Advanced Weka Segmentation" plug-in (which integrates a series of machine learning algorithms to learn the characteristics of nematodes on the same image for fast image segmentation) for ImageJ 1.48 software, imported experimental images and selected Gaussian blur, mean, Lipschitz, difference of Gaussians, variance and structure as image filters. After that, we manually outlined the worm contour as class 1, and the background was set to class 2, so as to train and adjust the image segmentation plug-in many times, relying on its powerful machine learning algorithm to distinguish nematodes and background. After training this model, we saved it and used it for all groups of image processing later. Since the body length of the nematode is much larger than its body width, we converted the body length of the nematode to 1/2 of the contour circumference under light stimulation. A worm was scored as dead if movement was less than 10%.[19] In terms of survival rate, we only evaluated the survival of adults. Using artificial correction, nematodes with a circumference of more than 2.0 mm are defined as adults were defined as adults, with the rest defined as larvae and eggs. The number of larvae and eggs of nematodes characterizes the parameter fecundity. Locomotion ability was assessed by calculating the distance moved by a nematode, by scanning the image twice. Comprehensive details regarding high-throughput phenotypic screening detection can be found in the Supporting Information (Text S3).

2.6. Statistical Analysis. GraphPad Prism 9.0 and Origin 2021 were used for the statistical analysis, and the findings are provided as mean values ± SD. An unpaired *t*-test was used to analyze the statistical significance of differences between two experimental groups, while a one-way ANOVA test was used to assess the significance of differences between three or more groups. The contribution weight and correlation of 15 PFAS to the four phenotypic parameters (growth, movement, survival and fecundity) of nematodes were analyzed by principal component analysis (PCA). Origin software (version 2022, Origin Lab Corp, USA) was used to perform PCA. For all statistical studies, the statistical significance level was fixed at 0.05.

3. RESULTS AND DISCUSSION

3.1. PFAS Screening and Identification. For suspect screening, we compiled and developed an in-house PFAS database. This database includes 18,603 PFAS and non-PFAS fluorinated species derived from the NORMAN Suspect List Exchange (https://www.norman-network.com/nds/SLE/) and the US EPA CompTox Chemistry Dashboard (https://comptox.epa.gov/dashboard/), as well as 6936 predicted MS/MS spectra. Using the nontargeted HPLC-MS analysis protocol and subsequent processes, a total of 3435 peaks were annotated by comparing the accurate mass in the in-house database with a 5 ppm variance. For nontarget screening, 5535 peaks remained after mass defect filtering

https://doi.org/10.1021/acs.est.4c03552
Environ. Sci. Technol. 2024, 58, 14530−14540

Class	No.	Formula	Theoretical mass[M-H]	Observed mass[M-H]	RT /min	Level
(1)	1	C4HF7O2	212.9792	212.9795	6.05	1
	2	C6HF11O2	312.9728	312.9732	10.42	1
	3	C7HF13O2	362.9696	362.9702	11.12	1
	4	C8HF15O2	462.9632	412.9669	11.59	1
	5	C9HF17O2	462.9632	462.9641	12.46	1
	6	C10HF19O2	512.9600	512.9604	13.14	1
	7	C11HF21O2	562.9568	562.9573	13.79	1
	8	C12HF23O2	612.9537	612.9544	14.43	1
	9	C13HF25O2	662.9505	662.9517	15.02	1
(2)	10	CHF3O3S	148.9526	149.0243	2.80	1
	11	C4HF9O3S	298.9430	298.9432	9.71	1
	12	C6HF13O3S	398.9366	398.9369	11.16	1
	13	C7HF15O3S	448.9334	448.9339	11.80	1
	14	C8HF17O3S	498.9302	498.9309	12.46	1
(3)	15	CH2F3NO2S	147.9686	147.9685	1.47	1
	16	C8H2F17NO2S	497.9462	497.9851	13.68	1
(4)	17	C2HF5O	134.9875	134.9875	12.01	2
(5)	18	C2H4F3NO2S	161.9842	161.9842	2.85	2
(6)	19	C3H6F3NO3S	191.9948	191.9947	2.18	2
(7)	20	C15H5F17O4S	602.9564	602.9571	16.48	2

Class	No.	Formula	Theoretical mass[M-H]	Observed mass[M-H]	RT /min	Level
(8)	21	C10H10F10O2	351.0448	351.0452	9.11	2
	22	C12H12F12O2	415.0573	415.0577	9.83	2
(9)	23	C10H2F18O2	494.9695	494.9702	11.77	3
	24	C12H2F22O2	594.9631	594.9640	12.90	3
	25	C14H2F26O2	694.9567	694.9577	14.09	3

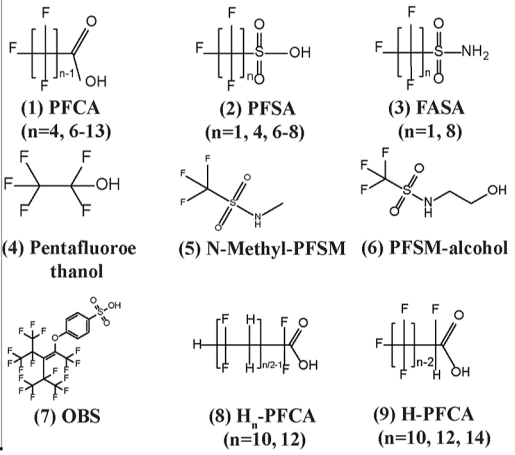

Figure 2. Proposed structure of legacy and emerging PFAS with level 3 or above identified by using suspect and nontarget analysis. Note: *n* is the number of all carbons in the PFAS.

and homologue detection. Finally, 2824 peaks were summarized as PFAS candidates using suspect and nontarget screening. Of these, 25 PFAS were identified at confidence level 3 or above, as listed in Figure 2, and categorized into nine classes. The term "legacy" typically refers to long-chain PFAS substances that have been well studied and widely present in the environment. Additionally, most of them have been phased out of production in numerous developed nations. Emerging PFAS includes not only alternatives to legacy PFAS substances, such as short-chain perfluorinated compounds and polyfluorinated alternatives, but also industrial byproducts and products degraded into novel PFAS.[20,21] Based on the above definition, the identified PFAS included 13 legacy PFAS (class 1, C7−C13; class 2, C6−C8; class 9, C10, C12, C14) and 12 emerging PFAS (class 1, C4, C6; class 2, C1, C4; classes 3−8) (Table S11). The Kendrick mass defect analysis gave the homologous series of peaks for perfluoroalkyl carboxylic acids (PFCAs), perfluoroalkyl sulfonic acids (PFSAs), hydrosubstituted-PFCAs (H-PFCAs), and perfluoroalkane sulfonamides (FASAs). An increasing RT trend with carbon chain length was found in each class of PFAS homologue (Figure S3).

3.1.1. PFCAs, PFSAs and FASAs. Several PFCA homologues (C4, C6−C13), five PFSA homologues (C1, C4, C6−C8), and two FASA homologues (C1 and C8) were detected through a combined approach of suspect and nontarget screening. In the case of PFCAs, their MS/MS spectra revealed a neutral loss of CO_2 (m/z 43.98) and fragments with the formula C_nF_{2n+1} (Figures S4−S12). The identification of PFSA structures relied on the presence of characteristic fragments at m/z 79.96 (SO_3), m/z 98.96 (SO_3F), and C_nF_{2n+1} fragments (Figures S13−S17). For FASAs, characteristic fragments at m/z 77.97 (SO_2N), m/z 63.96 (SO_2), and C_nF_{2n+1} fragments were observed in their MS/MS spectra (Figures S18 and S19). Confirmation of these compounds was achieved through comparison with authentic standards based on exact mass, RT, and MS/MS spectra (level 1).

3.1.2. Perfluorinated Alcohols. With a molecular formula of $[C_2F_5O]^-$ (5 ppm), the presence of the fragment 69.00 (CF_3) in the MS/MS spectrum indicates an oxygen atom at the end, leading to the classification of this class as perfluoroalkyl alcohols (PFAs) at level 2 (Figure S20).

3.1.3. Perfluoroalkyl Sulfonamides (PFSMs). Classes 5 and 6 were determined to be PFSMs following both suspect and nontarget screening processes, including compounds such as PFSM-alcohol and *N*-Methyl-PFSM. In the MS/MS spectra of PFSM-alcohol, the $[M\text{-}C_2H_5O]^-$ fragments were attributed to ethyl alcohol's neutral losses. Additionally, characteristic fragments at m/z 63.96 (SO_2) and 69.00 (CF_3) were observed, supporting the identification of PFSM-alcohol (level 2) (Figure S21). For *N*-Methyl-PFSM, characteristic fragments at m/z 63.96 (SO_2), 69.00 (CF_3), and 111.99 (CH_3FNO_2S) were present in its MS/MS spectra (level 2) (Figure S22).

3.1.4. P-perfluorous Nonenoxybenzenesulfonate (OBS). The molecular formula of the class 7 is $[C_{15}H_4O_4F_{17}S]^-$ (5 ppm), and was identified as OBS through a combined approach of suspect and nontarget screening. As indicated in the MS/MS spectrum of this class (Figure S23), the characteristic fragments at m/z 171.98 ($C_6H_4O_4S$), 348.98 ($C_{11}H_4O_3F_7S$), and 464.97 ($C_{13}H_4O_4F_{11}S$) were observed, in agreement with previous reports.[22]

3.1.5. Polyfluorocarboxylic Acids. Class 8 was recognized as polyfluorocarboxylic acids $C_{2n}H_{2n}F_{2n}O_2$ with a mass loss of 64 Da (CO_2HF) and a sequential loss of 20 Da (HF) in the MS/MS spectrum. The MS/MS fragment spectra of this class resembled those described by Charbonnet *et al.*[17] and Wei *et al.*[23] Consequently, two homologues were identified at level 2 based on the reported MS/MS spectrum in this class (Figure S24).

3.1.6. H-PFCAs. Three homologues were identified as hydrosubstituted-PFCAs. In the MS/MS spectrum (Figure S25), the $[M\text{-}64]^-$ fragment, corresponding to neutral losses of HF (20 Da) and CO_2 (44 Da), was observed across all masses

https://doi.org/10.1021/acs.est.4c03552
Environ. Sci. Technol. 2024, 58, 14530−14540

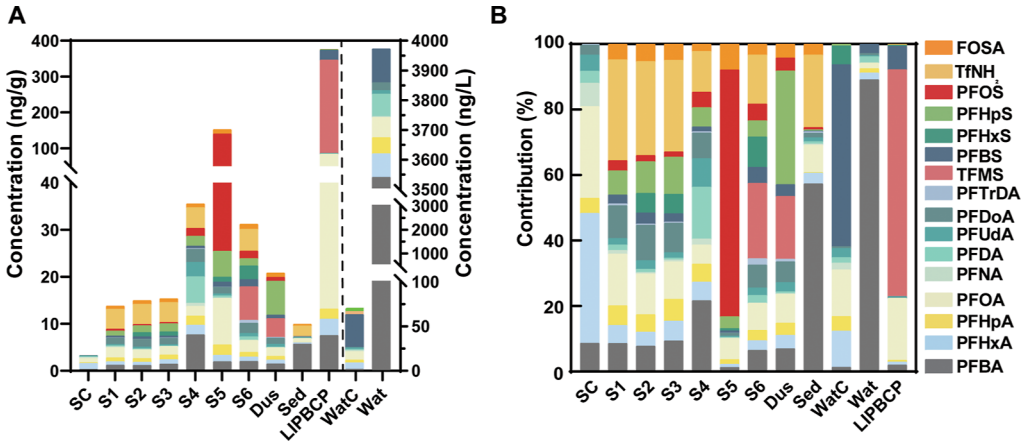

Figure 3. Occurrence and distribution of 16 target PFAS in different environmental media from the LIPB recycling area. (A) Concentration of 16 target PFAS in the soil, dust, sediment, LIPBCP and water collected from the LIPB recycling park and control area, (B) percentage of 16 target PFAS in the soil, dust, sediment, water and LIPBCP collected from the LIPB recycling park and control area.

Table 1. Concentration and Detection Rate of Target PFAS in the Soil, Dust, Water and Sediment Collected from the Studied LIPB Recycling Area

PFAS	soil (ng/g)							dust	sediment	water	LIPBCP	detection
	S1	S2	S3	S4	S5	S6	mean	(ng/g)	(ng/g)	(ng/L)	(ng/g)	rate (%)
PFBA	1.18	1.16	1.43	7.68	1.94	2.01	2.57	1.45	5.76	3537.07	7.50	100.0
PFHxA	0.76	0.64	0.93	2.01	1.36	0.93	1.10	0.85	0.32	79.48	3.48	100.0
PFHpA	0.82	0.79	1.02	1.96	2.24	0.98	1.30	0.78	0.02	54.27	2.15	100.0
PFOA	2.17	1.86	1.75	2.07	9.86	2.58	3.38	1.83	0.83	67.90	70.79	100.0
PFNA	0.15	0.07	0.09	0.66	0.10	0.01	0.18	0.03	0.03	2.90	0.16	100.0
PFDA	0.23	0.15	0.08	5.62	0.44	0.73	1.21	0.12	0.07	75.50	0.07	100.0
PFUdA	0.28	0.39	0.26	3.09	0.44	0.72	0.86	0.59	0.12	12.27	0.91	100.0
PFDoA	1.37	1.62	1.38	2.78	1.39	2.18	1.79	1.31	0.14	26.32	1.10	100.0
PFTrDA	0.08	0.05	0.05	0.14	0.05	0.60	0.16	0.17	0.04	n.d.	0.10	88.9
TFMS	n.d.[a]	n.d.	n.d.	n.d.	n.d.	7.17	7.17	3.98	n.d.	n.d.	259.75	22.2
PFBS	0.37	0.50	0.39	0.51	1.03	1.51	0.72	0.75	0.02	113.59	26.98	100.0
PFHxS	n.d.	0.90	0.91	n.d.	1.09	2.90	1.45	n.d.	n.d.	n.d.	1.13	44.4
PFHpS	1.02	1.44	1.73	2.10	5.48	1.54	2.22	7.20	0.04	n.d.	0.62	88.9
PFOS	0.43	0.29	0.25	1.67	114.47	1.59	19.78	0.83	0.07	n.d.	0.05	88.9
$TfNH_2$	4.23	4.28	4.28	4.43	n.d.	4.65	4.37	n.d.	2.19	n.d.	n.d.	66.7
FOSA	0.66	0.80	0.76	0.79	12.07	1.05	2.69	0.88	0.33	n.d.	0.84	88.9
$\sum_{16}$PFAS	13.77	14.94	15.31	35.51	151.93	31.16	43.77	20.78	9.88	3969.29	375.61	

[a]n.d. = not detected.

in class 9. Additionally, fragments at m/z 118.99 (C_2F_5) and m/z 168.99 (C_3F_7) resulting from the fluorocarbon chain break were detected in these classes, suggesting that the H atom is not at the chain's end. Although the loss of HF and C_nF_{2n-1} fragments in class 9 indicates the formation of a double bond with attached C atoms, the exact H-substitution position was not determined using MS/MS spectra, leading to the identification of this class at level 3.

Although there are no reports on the emission of, and pollution by PFAS at the LIPB recycling area, PFAS is undoubtedly an important manufacturing material for power batteries due to its excellent thermal stability and electrochemical properties. Most PFAS are used as ionic liquids in electrolytes and Zahn *et al.* found the release of TFMS from electrolytes to the environment.[24] In almost all commercial lithium-ion batteries, fluoropolymers such as polyvinylidene fluoride (PVDF) or propylene fluoride (FEP) are used as binder materials for anodes and cathodes. PVDF and FEP may produce highly fluorinated impurities in the production process, such as perfluorooctanoic acid (PFOA) and perfluorohexanoic acid (PFHxA), which belong to the substances of very high concern group. The impurities of these surfactants may remain in the binder material and be released during the cathode preparation process.[6] The incomplete combustion (temperature <850 °C) of fluorinated polymer cathode materials and fluorinated components in electrolytes may lead to the formation of various persistent PFAS. The potential pyrolysis products may be short-chain and long-chain perfluoroalkyl acids (PFAAs). The main use of perfluorononanoic acid (PFNA) is as a PVDF manufacturing aid; its use has been phased out in the United States. PVDF manufacturing additive Surflon S-111 contains high concentrations of PFNA, perfluoroundecanoic acid (PFUdA) and perfluorotridecanoic acid (PFTrDA).[25] Rensmo *et al.* summarized the possible fluorochemical emissions and pointed out that electrolytes and binders may be the main sources of PFAS emission at a LIPB recycling area.[6]

https://doi.org/10.1021/acs.est.4c03552
Environ. Sci. Technol. 2024, 58, 14530−14540

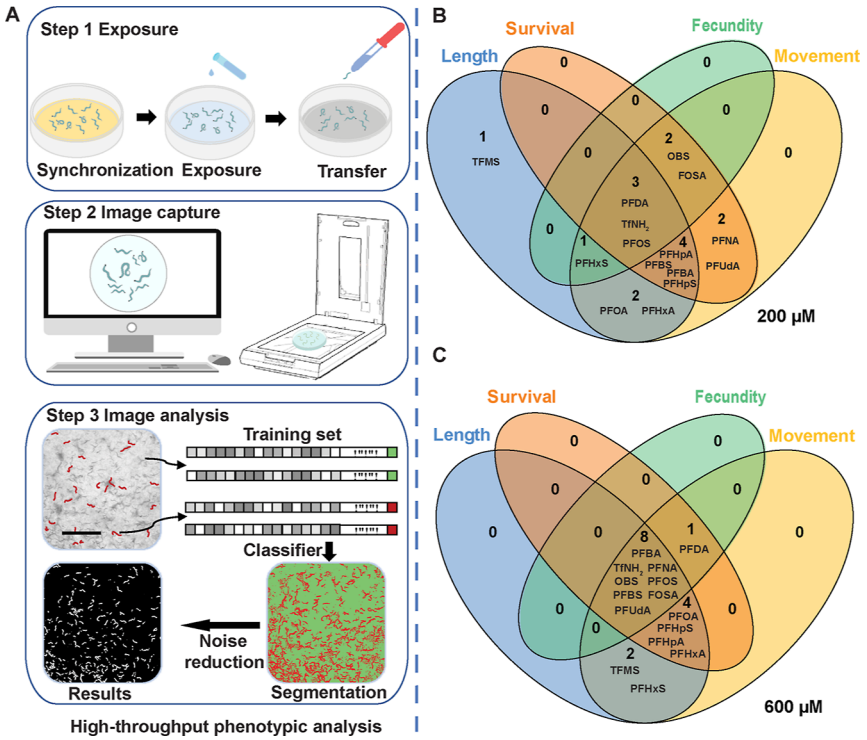

Figure 4. High-throughput phenotypic screening of PFAS by *C. elegans*. (A) Flow diagram of high-throughput phenotypic analysis of *C. elegans*, (B) Venn's diagram reporting the PFAS and their numbers with significant differences on the size, movement, survival and fecundity at 200 μM exposure level compared with the control group, (C) Venn's diagram reporting the PFAS and their numbers with significant differences on the size, movement, survival and fecundity at 600 μM exposure level compared with the control group.

3.2. Contamination Profiles of PFAS in the LIPB Recycling Area. The occurrence and distribution of screened PFAS seen using nontarget analysis in different environmental media from the LIPB recycling area studied were examined using target analysis. As shown in Figure 3 and Table 1, we selected a total of 16 PFAS for targeted analysis, and at least nine PFAS were detected in each environmental sample, indicating the widespread presence of PFAS in the LIPB recycling area. The detection rates in all collected environmental samples of perfluorobutanoic acid (PFBA), PFHxA, perfluoroheptanoic acid (PFHpA), PFOA, PFNA, perfluorodecanoic acid (PFDA), PFUdA, perfluorododecanoic acid (PFDoA), and perfluorobutanesulfonic acid (PFBS) were 100%, followed by PFTrDA, perfluoroheptanesulfonic acid (PFHpS), perfluorooctanesulfonic acid (PFOS), and perfluorooctane sulfonamide (FOSA) with a detection rate of 88.9%, $TfNH_2$ (66.7%), Perfluorohexanesulfonic acid (PFHxS) (44.4%) and TFMS (22.2%) (Tables 1 and S12). The Σ_{16}PFAS concentrations in the soil samples ranged from 13.77 to 151.93 ng/g, with an average of 43.77 ng/g. PFOS had the highest average concentration in the soil (0.25 ± 0.02−114.47 ± 27.36 ng/g, average of 19.78 ng/g) (Figure 3A, Tables 1 and S12). Of six soil collection sites, the soil sample (S5) taken from within the LIPB recycling area had the highest contamination level of all soil samples due to its high concentration of PFOS (114.47 ± 27.36 ng/g) (Figure 3A,B). As shown in Figure 3, PFBA, PFHxA, PFHpA, PFOA, PFUdA, PFDoA, PFTrDA, PFBS, PFHpS, $TfNH_2$, and FOSA were found in similar concentrations in the soil samples around the factory. However, the total concentration of PFAS in the depression soil samples was twice that of the soil at the outer edges of the other three plant areas, indicating that rainwater plays an important role in the diffusion and accumulation of regional PFAS.[26,27] Additionally, PFBA had a high concentration in the northwest puddled soil, sediment, and water samples (21.63, 57.37, 89.11%, respectively), while its concentration was low in other environmental samples (1.28 to 9.36%). This pattern is consistent with the behavior of many environmental contaminants, which are transported by water movement and eventually deposited in soil or sediment where they can concentrate.[28] On the other hand, PFBS had a very low concentration in all three samples (1.45, 0.16, 2.86%), possibly due to the hydrophilic nature of carboxylic functional groups compared to sulfonic functional groups, which hinder the movement of PFSAs in water.[29] The concentration range of $\sum_{16}$PFAS in soil samples was 13.77−151.93 ng/g, which was much higher than the total content of PFAS in agricultural soil samples in China (0.074−24.88 ng/g).[30] In terms of PFCA level in soil, the highest concentration was 9.86 ng/g in the S5 sample, surpassing the 6.8 ng/g of PFOA detected by Xu *et al.* in agricultural soil surrounding a fluorine chemical industrial park in China.[31] In an industrialized area of Sichuan Province, China, the concentration of $\sum_{10}$PFAS in soils was found to be 1.81 ng/g, while in our study, the concentration of the same 10 PFAS compounds was 147.56 ng/g, which represents an 81.5-fold increase in concentration.[32] Therefore, we believe that the spent LIPB recycling area may be another important source of PFAS pollution.

The $\sum_{16}$PFAS in dust was 20.78 ng/g, and the highest concentration was PFHpS (7.20 ± 0.21 ng/g). The sediment pollution was the smallest, and the total PFAS concentration was less than any other sample, only 9.88 ng/g (Table 1). The total concentration of PFAS in the wastewater from the site was 3969.29 ng/L, which was much lower than the

https://doi.org/10.1021/acs.est.4c03552
Environ. Sci. Technol. 2024, 58, 14530−14540

concentration in the wastewater (ranging from 5900 to 39,100 ng/L) from fluorochemical manufacturers, but significantly higher than the concentration in the wastewater treatment plant (ranging from 154.1 to 713.9 ng/L).[33−35] However, only nine PFAS were detected in wastewater, far fewer than in other water samples, indicating that the types of PFAS pollution at the power battery recycling area were still limited. It is worth noting that the PFAS detected in wastewater was mainly short-chain [PFCA (C4, C6) and PFSA (C4)], which was consistent with the findings of previous work.[34] The higher concentrations of short-chain PFAS in wastewater may be due to the stronger adsorption of long-chain PFAS by the factory wastewater treatment system as well as the transformation from long-chain PFAS to short-chain ones.

Notably, two ultrashort-chain PFAS, namely, TFMS (mean 5.58 ng/g, maximum 7.17 ± 0.00 ng/g, detection rate 22.2%) and $TfNH_2$ (mean 3.28 ng/g, maximum 4.65 ± 0.39 ng/g, detection rate 66.7%) were detected in multiple environmental media from the LIPB recycling area (Figure 3A, Tables 1 and S12). TFMS is known as a superacid and has important applications in electrochemistry as an electrolyte for energy storage and conversion devices such as lithium-ion batteries and fuel cells.[36] The concentration of TMFS in LIPBCP is also much higher than in environmental media (Tables 1 and S12). Additionally, among the 16 PFAS in our targeted analysis, $TfNH_2$ was the only substance not detected in LIPBCP. This means that $TfNH_2$ may not be directly released into the environment by LIPB disassembly. By comparing the chemical structure with the raw materials in the battery, we suspected that $TfNH_2$ might be a Lithium Bis(trifluoromethanesulfonyl)-imide (LiTFSI) degradation product or metabolite in the electrolyte. Further, the chemical metabolism simulator in OECD QSAR Toolbox Version 4.0 suggests that $TfNH_2$ is theoretically likely to be a biodegradable product of LiTFSI (Table S13).[37,38] However, the specific degradation characteristics and mechanisms need to be studied at more experimental levels.

3.3. High-Throughput Phenotypic Analysis. For this study, four phenotypic end points including growth, mortality, movement and fecundity of *C. elegans* were selected to screen the toxicity of 15 PFAS using automated high-throughput assaying (Figure 4, Table S14). Compared with the control group, PFDA, PFOS and $TfNH_2$ showed significant differences in the four phenotypic parameters of size, movement, survival and fecundity. The biplot relative to the first and second components is reported in Figure S26, where 15 target PFAS (points or scores) are distributed according to their phenotypic end points including growth, mortality, movement and fecundity of *C. elegans*. The cumulative explained variance of the first two PCs is 74.2%, and the PC1 alone provides the largest part, 52.8% of the total information. PCA analysis showed that PFDA, PFOS and $TfNH_2$ were the most toxic substances of all 15 PFAS with an exposure concentration of 200 μM (Figures 4B and S26, Table S14). PFDA belongs to the family of PFAS with ten carbon atoms and has been proven, using *in silico* methods including molecular docking, density functional theory and machine learning, to be the most toxic of common PFAS.[39] Moreover, recent studies using *in vitro* and *in vivo* biological models have found that PFDA is also one of the most significant PFAS in terms of reproductive development, cardiovascular and neurological toxicity.[40−42] Exposure to PFOS can cause multiple toxicities in laboratory animals and many *in vitro* human systems, such as reproductive and developmental toxicity, cardiovascular toxicity and neurotoxicity.[43,44] $TfNH_2$ is a representative substance of PFAS occurring in the LIPB recycling area. It is not only absent in existing reports on PFAS contamination at other typical industry sites, it may also be the degradation product of LiTFSI (a main raw material of LIPBs). At present, the research on the toxicity of $TfNH_2$ is extremely limited. However, $TfNH_2$ is a specific inhibitor of phospholipases A2, which can regulate cell function, inflammatory response and antibacterial activity by affecting arachidonic acid and lysophospholipid pathways.[45,46] The high toxicity of $TfNH_2$ suggests that we should not only pay attention to the traditional long-chain PFAS, but also pay special heed to the potential health hazards and challenges brought by ultrashort-chain PFAS in the health prevention and control research of PFAS.[47] Additionally, TFMS has the weakest toxic effect of all the detected PFAS, and only significantly affects the growth of nematodes, which may be related to its extremely short carbon chain (Figure 4B, Table S14).

When the exposure concentration increased to 600 μM, a total of eight PFAS compounds (PFBA, PFNA, PFUdA, $TfNH_2$, PFBS, PFOS, FOSA, OBS) that contained markedly adverse effects were screened (Figure 4B, Table S14). By integrating the above research results, our results suggest that we should not only scrutinize traditional highly toxic PFAS such as PFDA, PFOS, but also pay special attention to the potential health risks of LIPB-related specific ultrashort-chain PFAS ($TfNH_2$) in LIPB recycling areas.

It can be observed that the toxicity indexes of PFBA, PFBS, PFHpA and PFHpS (all short-chain PFAS) are consistent, indicating that the toxicities of short-chain carboxylic acid and sulfonic acid are similar, and have little effect on the reproduction of nematodes. It can be seen that PFHxS with the same carbon chain length has more significant toxicity indicators than PFHxA and PFOS compared with PFOA. This may be due to the fact that when the carbon chain length is the same, the sulfonic acid functional group has a greater effect on the toxicity of PFAS than the carboxylic acid functional group.[48] Survival rate is the most important indicator of the toxicity of reactive substances. PFHxS (C6) and PFHpS (C7) in sulfonic acid PFAS have only three significant indicators, but the survival rate of PFHxS (C6) is not significant, while the four toxicity indicators of PFOS (C8) are significant, which might suggest that longer carbon chain compounds exhibit higher toxicity than shorter carbon chain compounds.[49] As exposure concentration increases, the substances screened at 600 μM exposure level showed a significant increase in both quantity and toxicological effect intensity compared with those at 200 μM. At the same time, the linear growth in toxicity is also basically consistent with the previously reported rule that the toxicity increases with the increase in the length of carbon chains.[50] These results indicated that using high-throughput phenotypic analysis can quickly and accurately identify the *in vivo* toxic effects of various pollutants and the differences between them. In the past, the toxicity identification and screening of a large number of pollutants often required a lot of manpower, financial resources and time, especially when using *in vivo* models; the repeatability of data and the diversity of toxic effects were also unsatisfactory. In this study, we used *C. elegans* to identify and screen the *in vivo* toxicity of nontargeted screening substances, which not only provided new research ideas and techniques for the current high-throughput toxicological screening of pollutants but also provided a

https://doi.org/10.1021/acs.est.4c03552
Environ. Sci. Technol. 2024, 58, 14530−14540

guarantee for the verification and development of computational toxicology in the future.

In this study, 13 legacy and 12 emerging PFAS were screened out in multiple environmental media such as soil, dust, water and sediment by nontargeted detection, and their concentration and distribution characteristics in the environment were further clarified. Although this study revealed the pollution level and distribution characteristics of PFAS in a LIPB recycling area for the first time, the source, formation, migration and transformation mechanism of these PFAS still need to be further studied. In addition, by developing and improving the high-throughput phenotypic analysis, we carried out *in vivo* toxicological analysis of 15 PFAS found at the site. The results not only clarified the toxic effects of traditional long-chain PFAS on reproductive development, exercise, and survival, but also revealed the potential health risks and challenges of short-chain PFAS to site workers and surrounding populations. This project not only provides a scientific basis for the pollution prevention and control of PFAS at the LIPB recycling area and the healthy and green development of the industry, but also provides new research ideas and models for high-throughput identification and toxicity screening of pollutants in typical contaminated sites.

■ ASSOCIATED CONTENT

Supporting Information

The Supporting Information is available free of charge at https://pubs.acs.org/doi/10.1021/acs.est.4c03552.

Chemical reagents and sampling information; quality assurance and quality control (QA/QC); UHPLC-MS/MS detection conditions and parameter setting; the distinction between legacy and emerging PFAS; the concentration distribution of PFAS in each sample; biodegradable product of LiTFSI; nematode toxicity test results; battery recycling process; mass defects and RT versus numbers of fluorinated C atoms of PFAS (PDF)

■ AUTHOR INFORMATION

Corresponding Authors

Zongwei Cai − *Guangdong-Hong Kong-Macao Joint Laboratory for Contaminants Exposure and Health, School of Environmental Science and Engineering, Institute of Environmental Health and Pollution Control, Guangdong University of Technology, Guangzhou 510006, China; State Key Laboratory of Environmental and Biological Analysis, Department of Chemistry, Hong Kong Baptist University, Hong Kong 999077, China;* orcid.org/0000-0002-8724-7684; Phone: 852-34117070; Email: zwcai@hkbu.edu.hk; Fax: 852-34117348

Hemi Luan − *Department of Biomedical Engineering, School of Biomedical and Pharmaceutical Sciences, Guangdong University of Technology, Guangzhou 510006, China;* Email: luanhm@gdut.edu.cn

Authors

Zenghua Qi − *Guangdong-Hong Kong-Macao Joint Laboratory for Contaminants Exposure and Health, School of Environmental Science and Engineering, Institute of Environmental Health and Pollution Control, Guangdong University of Technology, Guangzhou 510006, China;* orcid.org/0000-0002-4611-8069

Yutian Cao − *Guangdong-Hong Kong-Macao Joint Laboratory for Contaminants Exposure and Health, School of Environmental Science and Engineering, Institute of Environmental Health and Pollution Control, Guangdong University of Technology, Guangzhou 510006, China*

Dan Li − *Guangdong-Hong Kong-Macao Joint Laboratory for Contaminants Exposure and Health, School of Environmental Science and Engineering, Institute of Environmental Health and Pollution Control, Guangdong University of Technology, Guangzhou 510006, China*

Chenguang Wu − *Guangdong-Hong Kong-Macao Joint Laboratory for Contaminants Exposure and Health, School of Environmental Science and Engineering, Institute of Environmental Health and Pollution Control, Guangdong University of Technology, Guangzhou 510006, China*

Kaihan Wu − *Guangdong-Hong Kong-Macao Joint Laboratory for Contaminants Exposure and Health, School of Environmental Science and Engineering, Institute of Environmental Health and Pollution Control, Guangdong University of Technology, Guangzhou 510006, China*

Yuanyuan Song − *State Key Laboratory of Environmental and Biological Analysis, Department of Chemistry, Hong Kong Baptist University, Hong Kong 999077, China*

Zeji Huang − *Guangdong-Hong Kong-Macao Joint Laboratory for Contaminants Exposure and Health, School of Environmental Science and Engineering, Institute of Environmental Health and Pollution Control, Guangdong University of Technology, Guangzhou 510006, China*

Xiaojing Meng − *Department of Occupational Health and Occupational Medicine, Guangdong Provincial Key Laboratory of Tropical Disease Research, School of Public Health, Southern Medical University, Guangzhou 510515, China*

Zhu Yang − *State Key Laboratory of Environmental and Biological Analysis, Department of Chemistry, Hong Kong Baptist University, Hong Kong 999077, China;* orcid.org/0000-0001-5934-1617

Complete contact information is available at: https://pubs.acs.org/10.1021/acs.est.4c03552

Author Contributions

Conceptualization was carried out by Z.H.Q., Z.W.C. and H.M.L. Methodology was carried out by Z.H.Q., Y.T.C., C.G.W., K.H.W., X.J.M.and Y.Y.S. Investigation was carried out by Z.H.Q., Y.T.C., C.G.W., K.H.W., Z.J.H., Z.Y. and H.M.L. Funding was acquired by Z.H.Q and Z.W.C. Supervision was carried out by Z.W.C. and Z.H.Q. Writing of the original draft was carried out by Z.H.Q and H.M.L, with additional writing, review, and editing carried out by Z.W.C., Z.H.Q. and H.M.L.

Notes

The authors declare no competing financial interest.

■ ACKNOWLEDGMENTS

This work was supported by the National Natural Science Foundation of China (42377419), the National Key Research and Development Project (2023YFC3905100), the General Research Fund from Hong Kong Research grants Council (12303320), Key R & D Plans of Guangzhou Science and Technology (202206010190) and the Guangdong-Hong Kong-Macao Joint Laboratory for Contaminants Exposure and Health (2020B1212030008).

REFERENCES

(1) Huang, J.; Dong, X.; Chen, J.; Zeng, A. The slow-release effect of recycling on rapid demand growth of critical metals from EV batteries up to 2050: Evidence from China. *Resour. Policy* **2023**, *82*, 103504.

(2) Proposal for a Regulation (EU) 2023/1542 of the European Parliament and of the Council of 12 July 2023. https://eur-lex.europa.eu/legal-content/EN/TXT/?uri=CELEX%3A32023R1542&qid=1705944298374 (accessed 01 29, 2024).

(3) Wu, S. B.; Kaden, N.; Dröder, K. A Systematic Review on Lithium-Ion Battery Disassembly Processes for Efficient Recycling. *Batteries* **2023**, *9* (6), 297.

(4) Mrozik, W.; Rajaeifar, M. A.; Heidrich, O.; Christensen, P. Environmental impacts, pollution sources and pathways of spent lithium-ion batteries. *Energ Environ. Sci.* **2021**, *14* (12), 6099−6121.

(5) Tian, G. D.; Yuan, G.; Aleksandrov, A.; Zhang, T. Z.; Li, Z. W.; Fathollahi-Fard, A. M.; Ivanov, M. Recycling of spent Lithium-ion Batteries: A comprehensive review for identification of main challenges and future research trends. *Sus tain Energy Technol. Assess* **2022**, *53*, 102447.

(6) Rensmo, A.; Savvidou, E. K.; Cousins, I. T.; Hu, X.; Schellenberger, S.; Benskin, J. P. Lithium-ion battery recycling: a source of per-and polyfluoroalkyl substances (PFAS) to the environment? *Environ. Sci. Process. Impacts* **2023**, *25*, 1015−1030.

(7) Gluge, J.; Scheringer, M.; Cousins, I. T.; DeWitt, J. C.; Goldenman, G.; Herzke, D.; Lohmann, R.; Ng, C. A.; Trier, X.; Wang, Z. An overview of the uses of per- and polyfluoroalkyl substances (PFAS). *Environ.Sci. Process. Impacts* **2020**, *22* (12), 2345−2373.

(8) Sauvé, S.; Barbeau, B.; Bouchard, M. F.; Verner, M.-A.; Liu, J. How Should We Interpret the New Water Quality Regulations for Per-and Polyfluoroalkyl Substances? *ACS ES & T Water* **2023**, *3* (9), 2810−2815.

(9) Hu, J.; Lyu, Y.; Chen, H.; Cai, L.; Li, J.; Cao, X.; Sun, W. Integration of target, suspect, and nontarget screening with risk modeling for per- and polyfluoroalkyl substances prioritization in surface waters. *Water Res.* **2023**, *233*, 119735.

(10) Zhao, M.; Yao, Y.; Dong, X.; Baqar, M.; Fang, B.; Chen, H.; Sun, H. Nontarget Identification of Novel Per- and Polyfluoroalkyl Substances (PFAS) in Soils from an Oil Refinery in Southwestern China: A Combined Approach with TOP Assay. *Environ. Sci. Technol.* **2023**, *57* (48), 20194−20205.

(11) Ghorbani Gorji, S.; Gomez Ramos, M. J.; Dewapriya, P.; Schulze, B.; Mackie, R.; Nguyen, T. M. H.; Higgins, C. P.; Bowles, K.; Mueller, J. F.; Thomas, K. V.; Kaserzon, S. L. New PFASs Identified in AFFF Impacted Groundwater by Passive Sampling and Nontarget Analysis. *Environ. Sci. Technol.* **2024**, *58* (3), 1690−1699.

(12) Wang, X.; Yu, N.; Qian, Y.; Shi, W.; Zhang, X.; Geng, J.; Yu, H.; Wei, S. Non-target and suspect screening of per- and polyfluoroalkyl substances in Chinese municipal wastewater treatment plants. *Water Res.* **2020**, *183*, 115989.

(13) Yu, N.; Guo, H.; Yang, J.; Jin, L.; Wang, X.; Shi, W.; Zhang, X.; Yu, H.; Wei, S. Non-Target and Suspect Screening of Per- and Polyfluoroalkyl Substances in Airborne Particulate Matter in China. *Environ. Sci. Technol.* **2018**, *52* (15), 8205−8214.

(14) Kim, S. W.; Song, W. Y.; Waldman, W. R.; Rillig, M. C.; Kim, T. Y. Toxicity of Aged Paint Particles to Soil Ecosystems: Insights from Caenorhabditis elegans. *Environ. Sci. Technol.* **2024**, *58* (1), 231−241.

(15) Hua, X.; Feng, X.; Liang, G. Y.; Chao, J.; Wang, D. Y. Exposure to 6-PPD Quinone at Environmentally Relevant Concentrations Causes Abnormal Locomotion Behaviors and Neurodegeneration in Caenorhabditis elegans. *Environ. Sci. Technol.* **2023**, *57* (12), 4940−4950.

(16) Loos, M.; Singer, H. Nontargeted homologue series extraction from hyphenated high resolution mass spectrometry data. *J. Cheminf.* **2017**, *9*, 12.

(17) Charbonnet, J. A.; McDonough, C. A.; Xiao, F.; Schwichtenberg, T.; Cao, D.; Kaserzon, S.; Thomas, K. V.; Dewapriya, P.; Place, B. J.; Schymanski, E. L.; Field, J. A.; Helbling, D. E.; Higgins, C. P. Communicating Confidence of Per- and Polyfluoroalkyl Substance Identification via High-Resolution Mass Spectrometry. *Environ. Sci. Technol. Lett.* **2022**, *9* (6), 473−481.

(18) Brenner, S. The genetics of Caenorhabditis elegans. *Genetics* **1974**, *77*, 71−94.

(19) Mathew, M. D.; Mathew, N. D.; Ebert, P. R. WormScan: a technique for high-throughput phenotypic analysis of Caenorhabditis elegans. *PLoS One* **2012**, *7* (3), No. e33483.

(20) Manojkumar, Y.; Pilli, S.; Rao, P. V.; Tyagi, R. D. Sources, occurrence and toxic effects of emerging per- and polyfluoroalkyl substances (PFAS). *Neurotoxicol. Teratol.* **2023**, *97*, 107174.

(21) Brase, R. A.; Mullin, E. J.; Spink, D. C. Legacy and Emerging Per- and Polyfluoroalkyl Substances: Analytical Techniques, Environmental Fate, and Health Effects. *Int. J. Mol.Sci.* **2021**, *22*, 995.

(22) Hou, M.; Jin, Q.; Na, G.; Cai, Y.; Shi, Y. Emissions, Isomer-Specific Environmental Behavior, and Transformation of OBS from One Major Fluorochemical Manufacturing Facility in China. *Environ. Sci. Technol.* **2022**, *56* (12), 8103−8113.

(23) Wang, Y.; Yu, N.; Zhu, X.; Guo, H.; Jiang, J.; Wang, X.; Shi, W.; Wu, J.; Yu, H.; Wei, S. Suspect and Nontarget Screening of Per- and Polyfluoroalkyl Substances in Wastewater from a Fluorochemical Manufacturing Park. *Environ. Sci. Technol.* **2018**, *52* (19), 11007−11016.

(24) Zahn, D.; Fromel, T.; Knepper, T. P. Halogenated methanesulfonic acids: A new class of organic micropollutants in the water cycle. *Water Res.* **2016**, *101*, 292−299.

(25) Prevedouros, K.; Cousins, I. T.; Buck, R. C.; Korzeniowski, S. H. Sources, fate and transport of perfluorocarboxylates. *Environ. Sci. Technol.* **2006**, *40* (1), 32−44.

(26) Wang, Q.; Guo, S.; Hou, Z.; Lin, H.; Liang, H.; Wang, L.; Luo, Y.; Ren, H. Rainfall facilitates the transmission and proliferation of antibiotic resistance genes from ambient air to soil. *Sci. Total Environ.* **2021**, *799*, 149260.

(27) Mahinroosta, R.; Senevirathna, L.; Li, M.; KrishnaPillai, K. A methodology for transport modelling of a contaminated site with perfluorooctane sulfonate due to climate interaction. *Process Saf. Environ. Prot.* **2021**, *147*, 642−653.

(28) Ahmed, M. B.; Johir, M. A. H.; McLaughlan, R.; Nguyen, L. N.; Xu, B.; Nghiem, L. D. Per- and polyfluoroalkyl substances in soil and sediments: Occurrence, fate, remediation and future outlook. *Sci. Total Environ.* **2020**, *748*, 141251.

(29) Eschauzier, C.; Beerendonk, E.; Scholte-Veenendaal, P.; De Voogt, P. Impact of treatment processes on the removal of perfluoroalkyl acids from the drinking water production chain. *Environ. Sci. Technol.* **2012**, *46* (3), 1708−1715.

(30) Wang, L.; Chen, L.; Wang, J.; Hou, J.; Han, B.; Liu, W. Spatial distribution, compositional characteristics, and source apportionment of legacy and novel per- and polyfluoroalkyl substances in farmland soil: A nationwide study in mainland China. *J. Hazard. Mater.* **2024**, *470*, 134238.

(31) Xu, K. R.; Huang, J.; Zhang, Y. F.; Wu, X. L.; Cai, D.; Hu, G. C.; Li, Y.; Ni, Z. B.; Lin, Q. Q.; Wang, S. Z.; Qiu, R. L. Crop Contamination and Human Exposure to Per- and Polyfluoroalkyl Substances around a Fluorochemical Industrial Park in China. *Toxics* **2024**, *12* (4), 269.

(32) Gan, C. D.; Peng, M. Y.; Liu, H. B.; Yang, J. Y. Concentration and distribution of metals, total fluorine, per- and poly-fluoroalkyl substances (PFAS) in vertical soil profiles in industrialized areas. *Chem.* **2022**, *302*, 134855.

(33) Zhang, Y.; Zhou, Y.; Dong, R.; Song, N.; Hong, M.; Li, J.; Yu, J.; Kong, D. Emerging and legacy per- and polyfluoroalkyl substances (PFAS) in fluorochemical wastewater along full-scale treatment processes: Source, fate, and ecological risk. *J. Hazard. Mater.* **2024**, *465*, 133270.

(34) Kim, J.; Xin, X. Y.; Mamo, B. T.; Hawkins, G. L.; Li, K.; Chen, Y. S.; Huang, Q. G.; Huang, C. H. Occurrence and Fate of Ultrashort-Chain and Other Per- and Polyfluoroalkyl Substances (PFAS) in Wastewater Treatment Plants. *ACS ES & T Water* **2022**, *2*, 1380−1390.

https://doi.org/10.1021/acs.est.4c03552
Environ. Sci. Technol. 2024, 58, 14530−14540

(35) Qiao, B. T.; Song, D. B.; Fang, B.; Yu, H.; Li, X.; Zhao, L. C.; Yao, Y. M.; Zhu, L. Y.; Chen, H.; Sun, H. W. Nontarget Screening and Fate of Emerging Per- and Polyfluoroalkyl Substances in Wastewater Treatment Plants in Tianjin, China. *Environ. Sci. Technol.* **2023**, *57* (48), 20127−20137.
(36) Bjornsdotter, M. K.; Yeung, L. W. Y.; Karrman, A.; Ericson Jogsten, I. Challenges in the analytical determination of ultra-short-chain perfluoroalkyl acids and implications for environmental and human health. *Anal. Bioanal. Chem.* **2020**, *412* (20), 4785−4796.
(37) Koleva, Y. Predicting the Microbial Activation of Some Perfluorinated Compounds. *J. Environ. Prot. Ecol.* **2021**, *22* (4), 1531−1540.
(38) Dimitrov, S. D.; Diderich, R.; Sobanski, T.; Pavlov, T. S.; Chankov, G. V.; Chapkanov, A. S.; Karakolev, Y. H.; Temelkov, S. G.; Vasilev, R. A.; Gerova, K. D.; Kuseva, C. D.; Todorova, N. D.; Mehmed, A. M.; Rasenberg, M.; Mekenyan, O. G. QSAR Toolbox - workflow and major functionalities. *SAR QSAR Environ. Res.* **2016**, *27* (3), 203−219.
(39) Duru, C. E. Forever chemicals could expose the human fetus to xenobiotics by binding to placental enzymes: Prescience from molecular docking, DFT, and machine learning. *Comput. Toxicol.* **2023**, *26*, 100274.
(40) Jane, L. E. L.; Yamada, M.; Ford, J.; Owens, G.; Prow, T.; Juhasz, A. Health-related toxicity of emerging per- and polyfluoroalkyl substances: Comparison to legacy PFOS and PFOA. *Environ. Res.* **2022**, *212*, 113431.
(41) Ojo, A. F.; Peng, C.; Ng, J. C. Assessing the human health risks of per- and polyfluoroalkyl substances: A need for greater focus on their interactions as mixtures. *J. Hazard. Mater.* **2021**, *407*, 124863.
(42) Ojo, A. F.; Peng, C.; Ng, J. C. Combined effects and toxicological interactions of perfluoroalkyl and polyfluoroalkyl substances mixtures in human liver cells (HepG2). *Environ. Pollut.* **2020**, *263*, 114182.
(43) Truong, L.; Rericha, Y.; Thunga, P.; Marvel, S.; Wallis, D.; Simonich, M. T.; Field, J. A.; Cao, D.; Reif, D. M.; Tanguay, R. L. Systematic developmental toxicity assessment of a structurally diverse library of PFAS in zebrafish. *J. Hazard. Mater.* **2022**, *431*, 128615.
(44) Zeng, Z.; Song, B.; Xiao, R.; Zeng, G.; Gong, J.; Chen, M.; Xu, P.; Zhang, P.; Shen, M.; Yi, H. Assessing the human health risks of perfluorooctane sulfonate by in vivo and in vitro studies. *Environ. Int.* **2019**, *126*, 598−610.
(45) Nakayama, H.; Ishihara, K.; Akiba, S.; Uenishi, J. Synthesis of N-[2-(2,4-Difluorophenoxy)trifluoromethyl-3-pyridyl]sulfonamides and Their Inhibitory Activities against Secretory Phospholipase A2. *Chem. Pharm. Bull.* **2011**, *59* (8), 1069−1072.
(46) Rayne, S.; Forest, K. A new class of perfluorinated acid contaminants: primary and secondary substituted perfluoroalkyl sulfonamides are acidic at environmentally and toxicologically relevant pH values. *J. Environ. Sci. Health, Part A: Toxic/Hazard. Subst. Environ. Eng.* **2009**, *44* (13), 1388−1399.
(47) Neuwald, I. J.; Hubner, D.; Wiegand, H. L.; Valkov, V.; Borchers, U.; Nodler, K.; Scheurer, M.; Hale, S. E.; Arp, H. P. H.; Zahn, D. Ultra-Short-Chain PFASs in the Sources of German Drinking Water: Prevalent, Overlooked, Difficult to Remove, and Unregulated. *Environ. Sci. Technol.* **2022**, *56* (10), 6380−6390.
(48) Feng, J.; Soto-Moreno, E. J.; Prakash, A.; Balboula, A. Z.; Qiao, H. Adverse PFAS effects on mouse oocyte in vitro maturation are associated with carbon-chain length and inclusion of a sulfonate group. *Cell Prolif.* **2023**, *56* (2), No. e13353.
(49) Cai, Y. P.; Chen, H. L.; Yuan, R. F.; Wang, F.; Chen, Z. B.; Zhou, B. H. Toxicity of perfluorinated compounds to soil microbial activity: Effect of carbon chain length, functional group and soil properties. *Sci. Total Environ.* **2019**, *690*, 1162−1169.
(50) Amstutz, V. H.; Cengo, A.; Gehres, F.; Sijm, D.; Vrolijk, M. F. Investigating the cytotoxicity of per- and polyfluoroalkyl substances in HepG2 cells: A structure-activity relationship approach. *Toxicology* **2022**, *480*, 153312.

https://doi.org/10.1021/acs.est.4c03552
Environ. Sci. Technol. 2024, 58, 14530−14540